Optimal Feedback Control of the Poloidal Magnetic Flux Profile in the DIII-D Tokamak Based on Identified Plasma Response Models

William Wehner, Wenyu Shi, Eugenio Schuster, Didier Moreau, Michael L. Walker, John R. Ferron, Tim C. Luce, David A. Humphreys, Ben G. Penaflor and Robert D. Johnson

***Abstract*— First-principles predictive models based on flux-averaged transport equations often yield complex expressions not suitable for real-time control implementations. It is however always possible to reduce these models to forms suitable for control design while preserving the dominant physics of the system. If further model simplification is desired at the expense of less model accuracy and controller capability, data-driven modeling emerges as an alternative to first-principles modeling. System identification techniques have the potential of producing low-complexity, linear models that can capture the system dynamics around an equilibrium point. This paper focuses on the control of the poloidal magnetic flux profile evolution in response to the heating and current drive (H&CD) systems and the total plasma current. Open-loop data for model identification is collected during the plasma current flattop in a high-confinement scenario (H-mode). Using this data a linear state-space plasma response model for the poloidal magnetic flux profile dynamics around a reference profile is identified. The control goal is to use the H&CD systems and the plasma current to regulate the magnetic profile around a desired target profile in the presence of disturbances. The target profile is defined close enough to the reference profile used for system identification in order to stay within the range of validity of the identified model. An optimal state feedback controller with integral action is designed for this purpose. Experimental results showing the performance of the proposed controller implemented in the DIII-D tokamak are presented.**

I. Introduction

To initiate a fusion reaction on earth, temperatures on the order of $10^7 - 10^9$ K are required to overcome the Coulomb repulsion between nuclei. The conventional fusion plasma, i.e., a hot gas of hydrogenic ions and electrons, must be confined by magnetic fields because the high temperatures would otherwise melt the confining structure. The ionized particles are tied to the magnetic field lines by the Lorentz force, limiting their motion to a helical path along the field lines, progressing linearly while gyrating in a circular orbit around the field lines. A magnetic field is thus capable of restricting the particle motion perpendicular to the field but does not prevent motion along the field lines. To limit the confinement to a bounded volume, the common solution is to close the magnetic field lines in on themselves, forming a torus. As shown in Fig. 1, the primary field component is the toroidal field B_ϕ. While moving along the field lines, the particles experience forces due to the curvature and gradient of the magnetic field causing outward drift and degrading confinement. This catastrophic effect can be avoided by twisting the field lines into a helical shape by adding a poloidal field component B_θ. A tokamak is a toroidal device in which the poloidal magnetic field is created by a toroidal current I_p flowing through the plasma. Following a given field line a number of times around the torus a closed flux tube is mapped, a so called magnetic-flux surface. Surfaces pertaining to different field lines form a set of nested surfaces around the torus axis. These surfaces are constant poloidal magnetic flux surfaces, where the poloidal magnetic flux at a point P in the (R, Z) cross section of the plasma is defined as the total flux through a circular surface centered on and perpendicular to the Z-axis and bounded by the toroidal ring passing through P [1]. Investigations have shown that careful control of some plasma profiles, including the poloidal magnetic flux profile, can help stabilize the plasma while reducing transport and enhancing non-inductive current sources necessary for steady-state operation [2], [3], [4] (we understand by profile the shape that a plasma variable takes as a function of the minor radius r (see Fig. 1)).

Mathematical modeling of plasma transport phenomena with sufficient complexity to capture the dominant dynamics is critical for plasma control design. Transport theories (classical, neoclassical and anomalous) even under restrictive assumptions, produce strongly nonlinear models based on partial differential equations (PDEs). The complexity of these first-principles models needs to be reduced for control design since it is very challenging, if not impossible, to synthesize compact and reliable control strategies based on these complicated mathematical models. During this control-oriented model reduction process there is always a trade-off between the simplicity of the model and both its physics accuracy and its range of validity, which will of course be reflected in the model-based controller performance and capability. First-principles modeling provides however the freedom of arbitrarily handling this trade-off and deciding on the level of simplicity, accuracy and validity of the model. If model simplicity is preferred over model accuracy and range of validity, data-driven modeling techniques, including system identification [5] and data assimilation [6], emerge as an alternative to first-principles modeling and have the potential to obtain low-complexity, linear, dynamic models useful for the design of local regulators around an equilibrium.

This work was supported by the National Science Foundation CAREER Award program (ECCS-0645086), the U.S. Department of Energy (DE-FG02-09ER55064, DE-FC02-04ER54698) and the European Communities under the contract of association between EURATOM and CEA (European Fusion Development Agreement). W. Wehner (wehner@lehigh.edu), W. Shi, and E. Schuster are with the Department of Mechanical Engineering and Mechanics, Lehigh University, Bethlehem, PA 18015, USA. D. Moreau is with CEA, IRFM, 13108 Saint-Paul-lez-Durance, France. M.L. Walker, J.R. Ferron, T.C. Luce, D.A. Humphreys, B.G. Penaflor, and R.D. Johnson are with General Atomics, San Diego, CA 92121, USA.

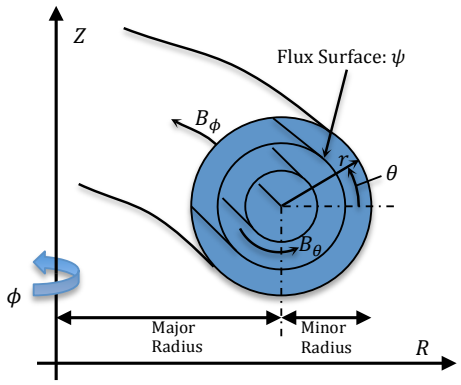

Fig. 1. Magnetic fields of a toroidal confinement system.

Data-driven modeling techniques have been successfully used in the past to model plasma transport dynamics for active control design in nuclear fusion reactors [7]. System identification using input/output data has been used to model the current profile dynamics in ASDEX Upgrade [8]. In the JET tokamak [9], a two-time-scale linear model has been used to describe the dynamics of the magnetic and kinetic profiles around certain quasi-steady-state trajectories, where system matrices can be identified from experimental data. In low confinement (L-mode) discharges of the JT-60U tokamak [10], diffusive and non-diffusive coefficients of the momentum transport equation of the toroidal rotation profile dynamics have been estimated from transient data obtained by modulating the momentum source.

This paper aims at developing an input-output response model, as well as a real-time feedback controller, for the magnetic profile dynamics (poloidal flux ψ relative to the boundary value) during H-mode scenarios in DIII-D. A linear time-invariant model is obtained using a system identification procedure described in Section II. As a result of this procedure, a model relating the poloidal magnetic flux profile to the neutral beams injectors (NBI), electron cyclotron (EC) H&CD, and the plasma current is obtained. Based on the linear model an optimal feedback integral controller is designed in Section III to regulate the ψ-profile around a desired target in the presence of disturbances. Experimental results on DIII-D are presented in Section IV. Finally, conclusions are stated in Section V.

II. System identification on DIII-D

By taking the average over the magnetic flux surfaces, plasma transport equations can be represented by one dimensional nonlinear parabolic PDEs whose variables are dependent on both time t and the normalized radius $\hat{\rho}$. The PDEs can be linearized around given trajectories as

$$\frac{\partial x(\hat{\rho},t)}{\partial t} = \mathcal{A}(\hat{\rho})x(\hat{\rho},t) + \mathcal{B}(\hat{\rho})u(t) + \mathcal{K}(\hat{\rho},t)e(\hat{\rho},t), \quad (1)$$

where $x(\hat{\rho},t)$ represents the collection of physical variables, e.g., the poloidal magnetic flux relative to the flux at the boundary, $\psi(\hat{\rho},t)$, in this work. The variable $u(t)$ represents the external control inputs including the total electron cyclotron power (EC) from all the gyrotrons, the neutral beam injection (NBI) power, and the plasma boundary surface loop voltage (V_{ext}) or alternatively the plasma current (I_p). The variables $\mathcal{A}(\hat{\rho})$, $\mathcal{B}(\hat{\rho})$, and $\mathcal{K}(\hat{\rho})$ are infinite dimensional operators. The system outputs $y(\hat{\rho},t)$ can be measured via various diagnostic systems

$$y(\hat{\rho},t) = \mathcal{C}(\hat{\rho})x(\hat{\rho},t) + e(\hat{\rho},t), \quad (2)$$

where $\mathcal{C}(\hat{\rho})$ is the observation operator and $e(\hat{\rho},t)$ is the observation noise field. The infinite dimensional system can be approximated by projecting the distributed variable $y(\hat{\rho},t)$ onto a Galerkin basis function space [11]. After the spatial discretization is achieved, the lumped parameter version of the infinite-dimensional state-space model (1)-(2) reads as

$$\frac{dX(t)}{dt} = AX(t)+Bu(t)+Ke(t); Y(t) = CX(t)+e(t), \quad (3)$$

where $X(t)$, $Y(t)$ are discrete-point vectors. Then we seek a least squares fit of the discrete model to experimental data.

To collect data for system identification a number of discharges of an advanced tokamak (AT) scenario (i.e., at high plasma pressure relative to the magnetic field pressure) were run with identical ramp-up phases [12]. Available neutral beam injectors and gyrotrons (EC power sources) were grouped to form, together with V_{ext}, five independent actuators: *i-* co-injection beam power (P_{CO}) *ii-* counter-injection beam power (P_{CNT}) *iii-* balanced-injection beam power (P_{BAL}) *iv-* total EC power from all gyrotrons in a fixed off-axis current drive configuration (P_{EC}), and *v-* V_{ext}. All actuators were modulated individually in open loop according to predefined waveforms while the other actuators were kept constant and equal to those values used to produce the reference discharge.

System identification for the poloidal flux profile $\psi_(\hat{\rho},t)$ was carried out for discrete points computed at normalized radii $\hat{\rho} = 0.2, 0.4, 0.5, 0.6,$ and, 0.8, in the time window $t = [2.6, 5.2]$ s. Although the system identification experiments were carried out in the loop voltage control mode, we have adopted the plasma current as system input instead of the loop voltage during the system identification procedure. We have decided to use the plasma current as a control input over the loop voltage simply because the DIII-D control system can provide far more accurate regulation of the plasma current. Fig. 2(a) shows a typical fit between the experimental data and the prediction by the identified model. The model prediction fits well all the shots, including those not used in the identification process such as shot 140094, which included modulation of all the actuators except the balanced-injection beam power. The fit between the original $Y(t)$ and reconstructed $Y_m(t)$ data is characterized by the parameter $f = 1 - \left[\frac{\sum_{k=1}^{N}[Y(t)-Y_m(t)]^2}{\sum_{k=1}^{N}[Y(t)-\langle Y\rangle]}\right]$, where $f = 1$ (100%) is a perfect fit and $f = 0$ corresponds to a reconstructed data set equal to the mean of the measured data, $\langle Y\rangle$.

Because we are interested in the slow dynamics (diffusion time-scale) of the magnetic variable ψ, the fast dynamics of both the inputs and ψ-profile were filtered out using Fast-Fourier Transform with a cut-off frequency of 4 Hz before identifying the model. The identification shots used to generate the model were then organized into various

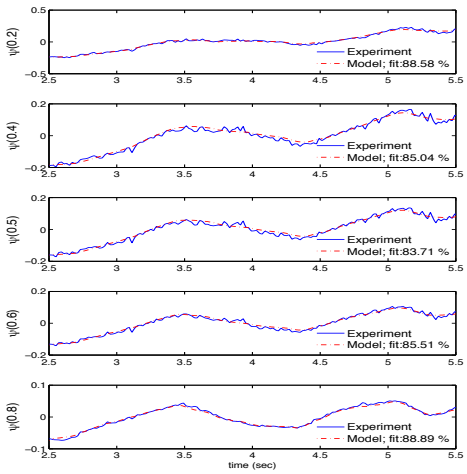

(a) Shot 140094

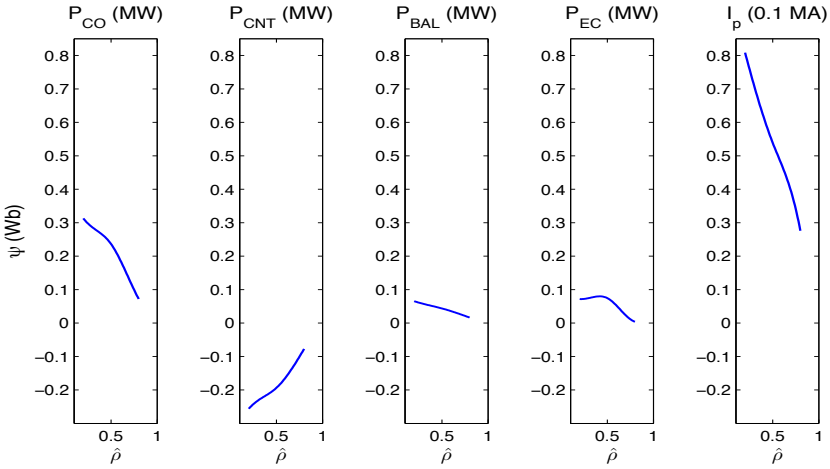

(b) Static gain

Fig. 2. Left: Comparison between measured (blue line) and estimated (red dash) of the ψ-profile (Wb) at $\hat{\rho} = 0.2, 0.4, 0.5, 0.6,$ and, 0.8 for DIII-D shot 140094. Right: Model steady-static gain matrix (static gain matrix). Each column represents the variation of the ψ-profile corresponding to a unit positive step variation of a given input. The powers are P_{CO} (MW), P_{CNT} (MW), P_{BAL} (MW), P_{EC} (MW), and I_p (0.1 MA).

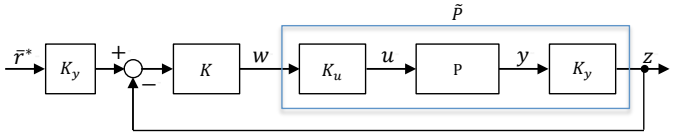

Fig. 3. Feedback scheme with SVD.

groups; one group for shots with very little modulation, and one group for each set of shots with modulation in just one of the actuators. The identification was then carried out in a stepwise fashion using the various shot groups to carry out the steps, following a procedure similar to that described in [12]. First, an initial estimation of the A matrix was determined using the shot group with very little or no modulation so that the slowest eigenmodes of the system could be estimated. Holding these eigenmodes constant, the columns of the B matrix were estimated in subsequent steps, one column at at time, using the shot group with modulation in the actuator corresponding to that column. The estimation process was carried out using the prediction error method [5] which calculates the matrices A and B by minimizing the norm $V_N(A,B) = \frac{1}{N}\sum_{k=1}^{N}\epsilon^2(k)$, where $\epsilon(k)$, called the prediction error, is the difference between the measured output and the predicted output at discrete time k.

The static gain matrix, $K_{sg} = -CA^{-1}B$, of the identified state space model can be represented as in Fig. 2(b). In the figure, the steady-state response of the poloidal flux to unitary changes in the various inputs of the model is plotted, where the powers are expressed in MW and the current in units of 0.1 MA. The plasma current is the most capable actuator in adjusting the magnetic profile in absolute terms. The co-injection and counter-injection beams are the second most powerful, affecting the profile in different directions. The contradictory effects of co-injection and counter-injection beams agree with prior experiments considering neutral beam injection at different trajectories [13]. Both the balanced-injection beams and the gyrotrons lead to a small increase in the magnetic flux profile.

III. Control System Structure

A. Control System Structure

The design of an optimal controller with integral action based on the linear data-driven model identified in Section II is presented in this section. The control algorithm is broken down into two steps: (1) decouple the system and reduce the system to the most relevant control channels (Section III-B) and (2) design the optimal controller based on the reduced system (Section III-C).

The particular plant model under consideration, labeled P, is of the form

$$P : \begin{cases} \dot{x} &= Ax + Bu \\ y &= Cx \end{cases} \tag{4}$$

where the model states represent the ψ-profile at the chosen discrete points and the output measurements y are identically the model states, i.e., $C = I_n$. The vectors $x(t)$, $u(t)$, and $y(t)$ are n-, m-, and p-order, state, control and output vectors, respectively.

B. Singular Value Decomposition

Singular value decomposition (Fig. 3) is employed to decouple the system and determine the most significant input-output channels for tracking. Provided the closed loop system is internally stable, the steady-state input-output relation can be described by the static gain matrix, $K_{sg} = -CA^{-1}B$,

$$\bar{y} = K_{sg}\bar{u}, \tag{5}$$

where $(\bar{\cdot})$ denotes the steady-state value. Consider the singular value decomposition of the weighted static gain matrix

$$\tilde{K}_{sg} = Q^{1/2}K_{sg}R^{-1/2} = U\Sigma V^T \tag{6}$$

where $\Sigma = diag(\sigma_1, \sigma_2, ..., \sigma_m) \in \mathbb{R}^{m\times m}$ for $m \leq p$, $U \in \mathbb{R}^{p\times m}$, $V \in \mathbb{R}^{m\times m}$, and σ_i are the individual singular values with $\sigma_1 > \sigma_2 > ... > \sigma_m$. The positive definite matrices $Q \in \mathbb{R}^{p\times p}$ and $R \in \mathbb{R}^{m\times m}$ are introduced to weight the

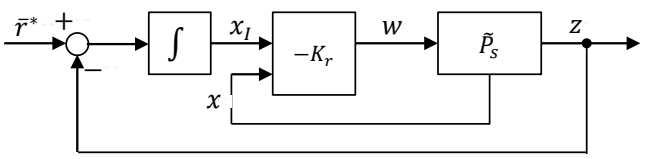

Fig. 4. LQR control configuration with integral action and reference input.

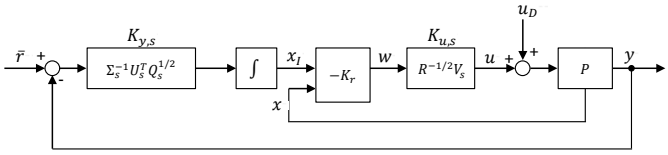

Fig. 5. Overall feedback scheme.

tracking error and steady-state control effort, respectively. Then the steady state output relation can be expressed as

$$\bar{y} = Q^{-1/2}\tilde{K}_{sg}R^{1/2}\bar{u} = Q^{-1/2}U\Sigma V^T R^{1/2}\bar{u}. \quad (7)$$

The columns of the matrix $Q^{-1/2}U\Sigma$ define a basis for subspace of obtainable steady state output values. Therefore the components of the output signal that are achievable can be defined as

$$\bar{z} = \Sigma^{-1}U^TQ^{1/2}\bar{y} \triangleq K_y\bar{y}. \quad (8)$$

Similarly, the components of the reference that are trackable can be expressed as

$$\bar{r}^* = \Sigma^{-1}U^TQ^{1/2}\bar{r} = K_y\bar{r}. \quad (9)$$

Making use of equations (5), (6) and (8)

$$\begin{aligned}\bar{z} &= \Sigma^{-1}U^TQ^{1/2}\bar{y}\\ &= \Sigma^{-1}U^TQ^{1/2}Q^{-1/2}U\Sigma V^TR^{1/2}\bar{u}\\ &= V^TR^{1/2}\bar{u} \triangleq K_u^{-1}\bar{u}.\end{aligned} \quad (10)$$

If we define $\bar{w} = V^TR^{1/2}\bar{u} = K_u^{-1}\bar{u}$ then we will have reduced the steady-state plant to a one-one relationship between inputs and outputs, i.e.,

$$\bar{z} = \bar{w}. \quad (11)$$

which represents a square $m \times m$ decoupled system. Let us define the steady-state performance index as

$$\bar{J} = \lim_{t\to\infty} e^T(t)Qe(t) = \bar{e}^TQ\bar{e}, \quad (12)$$

where $\bar{e}$ is the steady-state tracking error, which can now be rewritten as

$$\bar{e} = \bar{r} - \bar{y} = Q^{-1/2}U\Sigma(\bar{r}^* - \bar{z}) \quad (13)$$

and substituted into (12), resulting in the performance index

$$\bar{J} = (\bar{r}^* - \bar{z})^T\Sigma^2(\bar{r}^* - \bar{z}) = \sum_{i=1}^{m}\sigma_i^2(\bar{r}_i^* - \bar{z}_i)^2. \quad (14)$$

Clearly, the input-output channels associated with the largest singular values are the most significant when minimizing $\bar{J}$. Considering only the largest singular values and ignoring the others by reducing the system appropriately we can significantly reduce the control effort necessary to reach the steady-state target profile without substantial increase in the steady-state error [14]. The system is reduced to these important channels and the others are ignored. The reduction is carried out using the following partitions:

$$\begin{aligned}&U = [U_s \;\; U_{ns}],\;\; V = [V_s \;\; V_{ns}],\\ &\Sigma = \begin{bmatrix}\Sigma_s & 0\\ 0 & \Sigma_{ns}\end{bmatrix} \approx \begin{bmatrix}\Sigma_s & 0\\ 0 & 0\end{bmatrix},\end{aligned} \quad (15)$$

where s stands for significant and *ns* stands for non-significant. Then, from (7), we can approximate

$$\bar{y} = Q^{-1/2}U\Sigma\bar{z} \approx Q^{-1/2}U_s\Sigma_s\bar{z} \triangleq K_{y,s}^{-1}\bar{z}, \quad (16)$$

$$\bar{w} = V^TR^{1/2}\bar{u} \approx V_s^TR^{1/2}\bar{u} \triangleq K_{u,s}^{-1}\bar{u}. \quad (17)$$

Defining $z = K_{y,s}y$ and $u = K_{u,s}w$, we can write

$$z = K_{y,s}PK_{u,s}w \triangleq \tilde{P}_sw, \quad (18)$$

where we have used the fact that $y = Pu$, $K_{y,s} = \Sigma_s^{-1}U_s^TQ^{1/2}$ and $K_{u,s} = R^{-1/2}V_s$. The reduced plant is characterized by the state space representation

$$\tilde{P}_s : \left\{\begin{array}{rcl}\dot{x} &=& \tilde{A}x + \tilde{B}w\\ z &=& \tilde{C}x\end{array}\right. \quad (19)$$

where $\tilde{A} = A$, $\tilde{B} = BK_{u,s}$ and $\tilde{C} = K_{y,s}C$.

C. Optimal State Feedback Controller

The control design considers an optimal state feedback controller with integral action added as shown in Fig. 4 to remove the steady-state error. Here the control error $\bar{r}^* - z$ is integrated and the controller is designed for the augmented plant with the integrator states. Adding the integrator states, $x_I = \int \bar{r}^* - z$, to the reduced plant $\tilde{P}$, the augmented plant $(\hat{A}, \hat{B})$ can be expressed as:

$$\dot{\hat{x}} = \begin{bmatrix}0 & -\tilde{C}\\ 0 & \tilde{A}\end{bmatrix}\hat{x} + \begin{bmatrix}-\tilde{D}\\ \tilde{B}\end{bmatrix}w + \begin{bmatrix}1\\ 0\end{bmatrix}\bar{r}^* \quad (20)$$

with augmented states $\hat{x} = \begin{bmatrix}x_I\\ x\end{bmatrix}$.

The task of the control synthesis is to find the optimal control law $w(t) = f(\hat{x}(t))$ which minimizes the cost functional

$$J = \lim_{T\to\infty}\frac{1}{T}\int_0^T \left[\hat{x}^T\hat{Q}\hat{x} + w^T\hat{R}w\right]dt, \quad (21)$$

where $\hat{Q}$ is a $n \times n$ symmetric positive-semidefinite matrix and $\hat{R}$ is a $m \times m$ symmetric positive-definite matrix [15]. The solution to this linear quadratic regulator problem (LQR) can be written in terms of the simple state feedback law

$$w(t) = -K_r\hat{x}(t) \quad (22)$$

where K_r is a constant matrix independent of plant noise, given by

$$K_r = \hat{R}^{-1}\hat{B}^TX, \quad (23)$$

where $X = X^T \geq 0$ is the unique positive-semidefinite solution of the algebraic Riccati equation

$$\hat{A}^TX + X\hat{A} - X\hat{B}\hat{R}^{-1}\hat{B}^TX + \hat{Q} = 0. \quad (24)$$

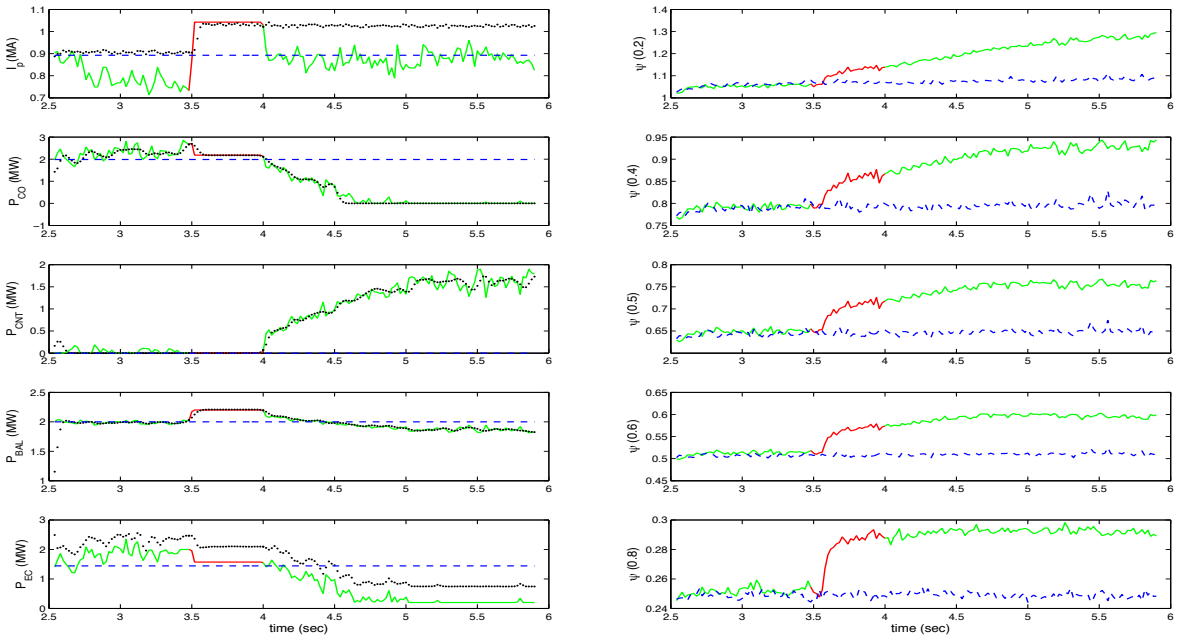

(a) Inputs (b) ψ

Fig. 6. Shot #146456: The blue dashed line represents the reference profile and associated inputs. The red and green lines represent the requested inputs and measured ψ-profile. The red portion denotes a period of no feedback. The black dotted line represents the actual delivered inputs.

We choose $\hat{Q}$ such that only the integrated states $\int \bar{r} - y$ are weighted, which gives $\hat{Q} = \begin{bmatrix} I_n & 0 \\ 0 & 0 \end{bmatrix}$, and we choose $\hat{R} = \alpha I_m$, with $\alpha > 0$. Note that only the ratio between $\hat{R}$ and $\hat{Q}$ affects the minimum of the cost function, reducing $\hat{R}$ yields a faster response with more control energy.

The control configuration of Fig. 4 can be re-expressed in the form of Fig. 5 to determine the overall controller. The result is the two degree of freedom controller $\tilde{K}$. Using the relation

$$w = -K_r \begin{bmatrix} x_I \\ x \end{bmatrix} \triangleq \begin{bmatrix} -K_I & -K_P \end{bmatrix} \begin{bmatrix} x_I \\ x \end{bmatrix}, \qquad (25)$$

and absorbing the integrator, $\tilde{K}$ can be written as

$$\tilde{K} : \begin{cases} \dot{x}_I &= 0x_I + \begin{bmatrix} K_{y,s} & -K_{y,s} \end{bmatrix} \begin{bmatrix} \bar{r} \\ y \end{bmatrix}, \\ u &= -K_{u,s} K_I x_I - K_{u,s} \begin{bmatrix} 0 & K_P \end{bmatrix} \begin{bmatrix} \bar{r} \\ y \end{bmatrix}, \end{cases} \qquad (26)$$

where K_I is the state feedback matrix for the integrated states and K_P is the state feedback for the original states.

IV. Experimental Results

Using the identified model of Section II, the proposed optimal control law synthesized in Section III was put to the test in experiments on DIII-D. The first two singular values are found to be the most significant and the system is reduced to 2×2 in the singular value decomposition. The weight $\hat{Q}$ is selected such that only the integrator states are weighted in the control design and α is selected such that the system reacts sufficiently quickly without too much overshoot. During the experiment the device was setup to reproduce the initial ramp-up profile of the reference discharge used in section II for system identification.

Some tuning was done in simulation and eventually the SVD weighting matrices were selected as $Q = diag\{10\}$, $R = diag\{100, 1, 1, 1, 1\}$. This first value of 100 for R was selected to reduce the control effort applied to the plasma current, this large value was chosen to make sure the actuator did not bounce between saturation limits in simulation. The multiplier α was set to 0.01 for the controller weight $\hat{R}$. Fig. 6 shows the resulting inputs and outputs (ψ-profile evolution) of the experimental shot #146456. From 2.5 to 3.5 s the control performs well, holding the ψ-profile tight with the desired target. It is also clear from Fig. 6(a) that the controller is indeed functioning, the actuators are moving significantly and not just following the feed-forward values of the reference discharge. At 3.5 s an input disturbance (0.15MA on I_p, 0.2MW on P_{CO}, 0.2 MW on P_{BAL}, and 0.13 MW on P_{EC}) is applied through the PCS (denoted by u_d in Fig. 5) and the feedback is turned off for 0.5 s to allow the disturbance to perturb the system. At 4 s the feedback is turned back on at which point the controller quickly reacts to the disturbance. However, after 4 s the delivered I_p fails to follow the requested value, i.e., the black dots remain around 1.1 while the requested value is around 0.9. This problem was due to a wrong setup in the I_p dedicated current controller. The error in I_p then causes the ψ-profile to further diverge from the desired target. It is quite clear, however, that the controller is moving the neutral beams and the gyrotron powers in the correct direction; saturating the co-current and balanced beams and the gyrotrons at zero power, and saturating the counter-current beam at maximum power, all of which are desired to decrease the profile values.

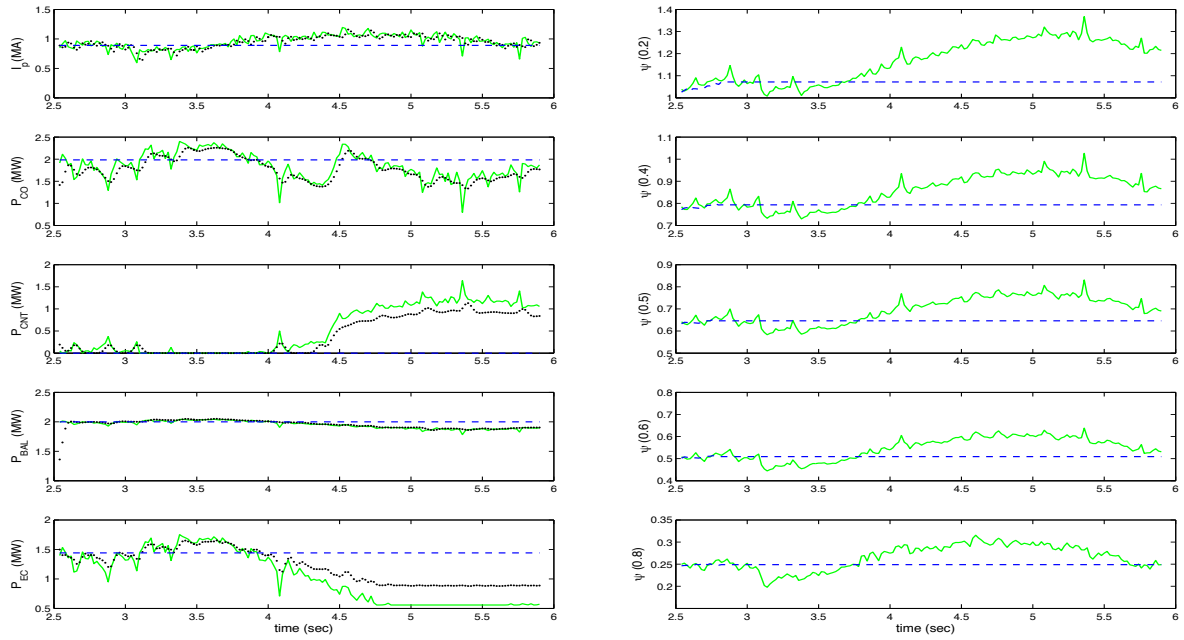

(a) Inputs (b) ψ

Fig. 7. Shot #147705: The blue dashed line represents the reference profile and associated inputs. The green line represents the requested inputs and the measured ψ-profile. The black dotted line represents the actual delivered inputs.

In the second experiment the large weight on I_p used in R was reduced to 10, i.e., $R = diag\{10, 1, 1, 1, 1\}$, $Q = diag\{10\}$. In addition, α was increased to 0.1. The experimental implementation of this controller in shot #147705 is illustrated in Fig. 7. A disturbance of -0.1 MA is added to I_p at $t = 3$ s and disturbances of 1 MW and 0.5 MW are added to the co-injection beams and the counter-injection beams, respectively, at $t = 4.5$ s. There is no significant discrepancy between requested and delivered inputs throughout the discharge, with the exception of a small offset in requested P_{EC}. The control performance is rather sluggish, probably due to the reduction in α. The ψ profile fall below the target value after the disturbance in I_p is introduced at $t = 3$ s. The controller reacts to this induced tracking error but producing an overshoot that is not corrected until the end of the discharge when the ψ profile seems to converge back to the target value. More experimental time seems to be necessary to appropriately tune the controller weights and gains.

V. Conclusions

A simplified linear model for the evolution of the poloidal magnetic flux profile in DIII-D was obtained based on system identification methods. Reasonable model prediction of the magnetic profile evolution in response to modulations in the neutral beam injector power, the total gyrotron power, and the plasma current was achieved. An optimal feedback controller with integral action was proposed for tracking a desired target profile. Sufficient profile control in the presence of disturbances was verified in simulations and encouraging preliminary results were obtained in experiment. It is suspected that improved closed-loop performance can be achieved by further tuning of the control parameters.

References

[1] A. Pironti and M. Walker, "Fusion, tokamaks, and plasma control," *IEEE Control System Magazine*, vol. 25, no. 5, pp. 30–43, 2005.

[2] F. Romanelli and R. Kamendje, "Overview of JET results," *Nucl. Fusion*, vol. 49, no. 104006, 2009.

[3] N. Oyama and for the JT-60 Team, "Overview of JT-60U results towards the establishment of advanced tokamak operation," *Nucl. Fusion*, vol. 49, no. 104007, 2009.

[4] E. Strait and for the DIII-D Team, "DIII-D research in support of ITER," *Nucl. Fusion*, vol. 49, no. 104008, 2009.

[5] L. Ljung, *System Identification: Theory for the User*. Prentice Hall PTR, 1999.

[6] B. Anderson and J. Moore, *Optimal Filtering*. Prentice Hall, 1979.

[7] P. Wang, *Distributed Parameter Systems: Modelling and Identification*. Berlin, Germany: Springer-Verlag, 1978.

[8] Y. S. Na, "Modelling of current profile control in tokamak plasmas," Ph.D. dissertation, Fakultat fur Physik: Technische Universitat Munchen, Munich, Germany, 2003.

[9] D. Moreau *et al.*, "A two time scale dynamic model approach for magnetic and kinetic profile control in advanced tokamak scenarios on JET," *Nucl. Fusion*, vol. 48, no. 106001, 2008.

[10] Y. Yoshida *et al.*, "Momentum transport and plasma rotation profile in toroidal direction in JT-60U L-mode plasmas," *Nucl. Fusion*, vol. 47, no. 8, pp. 856–863, 2007.

[11] W. Wehner *et al.*, "Data-driven modeling and feedback tracking control of the toroidal rotation profile for advanced tokamak scenarios in DIII-D," *Proceedings of the 2011 IEEE Multiconference on Systems and Control*, 2011.

[12] D. Moreau *et al.*, "Plasma models for real-time control of advanced tokamak scenarios," *Nucl. Fusion*, vol. 51, no. 063009, 2011.

[13] W. Heidbrink *et al.*, "Beam-ion confinement for different injection geometries," *Plasma Physics and Controlled Fusion*, vol. 51, no. 125001, 2009.

[14] G. Ambrosino, M. Ariola, and A. Pironti, "Optimal steady-state control for linear non right-invertible systems," *IET Control Theory and Applications*, vol. 1, no. 3, pp. 604–610, 2007.

[15] S. Skogestad and I. Postlethwaite, *Multivariable Feedback Control*. John Wiley & Sons, West Sussex England, 2005.